Performance comparison of ghost imaging versus conventional imaging in photon shot noise cases

Zijie Li (李自杰)[1], Qing Zhao (赵 清)[1,*], and Wenlin Gong (龚文林)[2,]**

[1]*Center for Quantum Technology Research, School of Physics, Beijing Institute of Technology, Beijing 100081, China*
[2]*Key Laboratory for Quantum Optics and Center for Cold Atom Physics of CAS, Shanghai Institute of Optics and Fine Mechanics, Chinese Academy of Sciences, Shanghai 201800, China*
**Corresponding author: qzhaoyuping@bit.edu.cn; **corresponding author: gongwl@siom.ac.cn*
Received November 20, 2019; accepted April 16, 2020; posted online May 22, 2020

The performances of ghost imaging and conventional imaging in photon shot noise cases are investigated. We define an imaging signal-to-noise ratio called $\mathrm{SNR}^{\mathrm{tran}}$ where only the object's transmission region is used to evaluate the imaging quality and it can be applied to ghost imaging (GI) with any random pattern. Both the values $\mathrm{SNR}_{\mathrm{GI}}^{\mathrm{tran}}$ of GI and $\mathrm{SNR}_{\mathrm{CI}}^{\mathrm{tran}}$ of conventional imaging in photon shot noise cases are deduced from a simple statistical analysis. The analytical results, which are backed up by numerical simulations, demonstrate that the value $\mathrm{SNR}_{\mathrm{GI}}^{\mathrm{tran}}$ is related to the ratio between the object's transmission area A_o and the number density of photons illuminating the object plane I_o, which is similar to the theoretical results based on the first principle of GI with a Gaussian speckle field deduced by B. I. Erkmen and J. H. Shapiro [in Adv. Opt. Photonics 2, 405–450 (2010)]. In addition, we also show that the value $\mathrm{SNR}_{\mathrm{CI}}^{\mathrm{tran}}$ will be larger than $\mathrm{SNR}_{\mathrm{GI}}^{\mathrm{tran}}$ when A_o is beyond a threshold value.

Keywords: ghost imaging; photon shot noise; signal-to-noise ratio; speckle.
doi: 10.3788/COL202018.071101.

Ghost imaging (GI), as a nonlocal imaging method, can image an unknown object with a single-pixel detector at the object path[1–6]. In the most recent two decades, GI has been receiving increasing interest and lots of achievements have been made, especially in the fields of remote sensing[7–9], X-ray microscopy[10,11], three-dimensional imaging[12,13], and super-resolution imaging[14–16]. The feasibility of GI has also been experimentally demonstrated[7–20] from X-rays to microwave sources. However, there is still a long way to go for the practical application of GI, because some issues like imaging speed and moving target imaging without the prior knowledge of motion feature have not been solved and some physical mechanisms have not been clarified up to now. For example, for conventional imaging (CI), the imaging signal-to-noise ratio (SNR) is the same as the detection SNR. However, when the intensity of light illuminating the object plane is the same, the detection SNR of GI increases with the object's transmission area because all the photons transmitted from the object illuminate the same single-pixel detector, but the imaging SNR of GI is reduced and is also related to the property of random coded patterns illuminating the object[5,21–23], which is entirely different from CI. It is natural to ask what the quantitative relationship between the detection SNR and the imaging SNR of GI is. Although Erkmen and Shapiro have done some theoretical analysis on factors affecting the imaging SNR of GI, it was only applied to the random coded patterns with the Gaussian statistical property and the computation of the imaging SNR is relative complicated[22]. Can we propose a new imaging SNR for GI that is used for any random patterns with different statistical properties and is easy to compute? For another example, the photon shot noise, which is the main factor affecting the imaging SNR of CI, will cause the detection signal's intensity fluctuation, and thus it also affects the imaging SNR of GI due to the object's information extraction that originates from the intensity fluctuation correlation of light fields for GI. It is natural to ask what conditions should be satisfied if GI is better than CI in photon shot noise cases. In this Letter, we propose an imaging SNR called $\mathrm{SNR}^{\mathrm{tran}}$ to evaluate the imaging quality of both GI and CI. Based on the deduced $\mathrm{SNR}^{\mathrm{tran}}$, the influences of some parameters like the photon shot noise, the object's transmission area, and the number density of photons illuminating the object plane on the imaging quality of GI are clarified, and the performance differences between CI and GI are also discussed by theoretical analysis and numerical simulations.

Figure 1(a) presents a typical schematic of computational GI. The light emitted from a pulsed laser uniformly illuminates a digital micro-mirror device (DMD) and a series of random coded patterns are prebuilt by modulating the mirrors of the DMD. Then the patterns reflected by the DMD are imaged onto an object by an optical imaging system with the focal length f_t, and the photons transmitted through the object are imaged onto a bucket detector D_t by using another conventional imaging system with the focal length f_r. In comparison with Fig. 1(a), a conventional imaging setup is shown in Fig. 1(b), where the DMD and the bucket detector D_t are replaced by a reflection mirror and a CCD camera, respectively.

In the framework of computational GI, the object's image O_{GI} can be reconstructed by computing the intensity correlation between the pattern's intensity $I_r^s(x,y)$ modulated by the DMD and the total intensity I_B^s recorded by the bucket detector D_t[6],

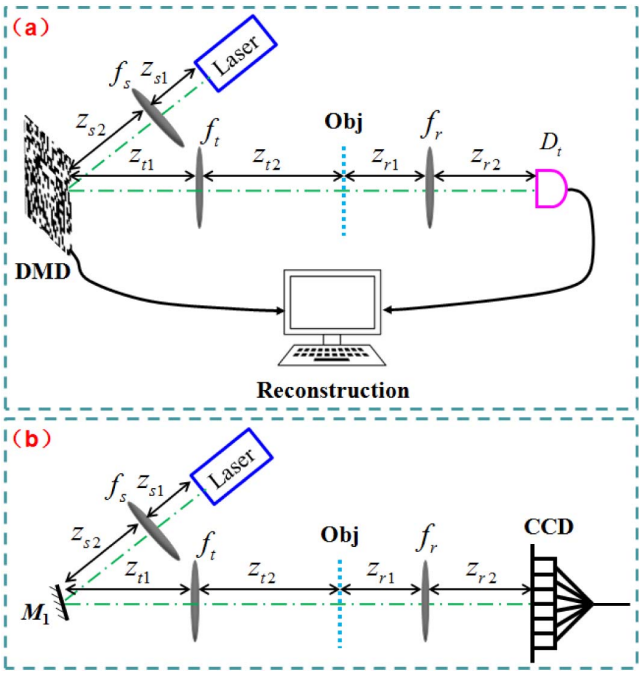

Fig. 1. Typical schematics of (a) computational GI and (b) CI via laser illumination.

$$O_{\mathrm{GI}}(x,y)=\frac{1}{K}\sum_{s=1}^{K}[I_r^s(x,y)-\langle I_r^s(x,y)\rangle]I_B^s$$
$$=\frac{1}{K}\sum_{s=1}^{K}\Delta I_r^s(x,y)I_B^s, \tag{1}$$

where s denotes the sth measurement and K is the total measurement number. In addition, $\langle I_r^s(x,y)\rangle=\frac{1}{K}\sum_{s=1}^{K}I_r^s(x,y)$ represents the ensemble average of $I_r^s(x,y)$, and $\Delta I_r^s(x,y)=I_r^s(x,y)-\langle I_r^s(x,y)\rangle$ is the intensity fluctuation of $I_r^s(x,y)$.

When the numerical aperture of the lens with a focal length f_r shown in Fig. 1(a) is large enough, and considering the photon shot noise of the detection system, the total intensity I_B^s can be expressed as

$$I_B^s=I_{\mathrm{signal}}^s+I_{\mathrm{noise}}^s,\quad \forall_s=1,2,...,K, \tag{2}$$

where $I_{\mathrm{noise}}^s=\iint \mathrm{d}x\mathrm{d}yI_r^s(x,y)O(x,y)$ and $O(x,y)$ is the object's transmission function. In addition, $I_{\mathrm{noise}}^s=\mathrm{Poisson}(I_{\mathrm{signal}}^s)-I_{\mathrm{signal}}^s$ and $\mathrm{Poisson}(I_{\mathrm{signal}}^s)$ represents the Poisson distribution with the mean value I_{signal}^s.

For the setup of GI displayed in Fig. 1(a), the bucket detector D_t collects all the photons transmitted through the object. If only considering the photon shot noise of the detection system, the detection signal-to-noise ratio (DSNR) of GI can be represented as

$$\mathrm{DSNR}_{\mathrm{GI}}=10\times\log_{10}\left[\frac{\langle I_{\mathrm{signal}}^s\rangle}{\mathrm{std}(I_{\mathrm{noise}}^s)}\right]\approx 10\times\log_{10}\left(\sqrt{\langle I_{\mathrm{signal}}^s\rangle}\right)$$
$$=10\times\log_{10}\left(\sqrt{I_oA_o}\right), \tag{3}$$

where $I_o=\langle I_r^s(x_0,y_0)\rangle$ is the average number density of photons illuminating the object plane, the quantum efficiency of the detector is assumed to be 1, and $A_o=\iint \mathrm{d}x\mathrm{d}yO(x,y)$ is the transmission area of the object. In addition, $\langle I_{\mathrm{signal}}^s\rangle=I_o\iint \mathrm{d}x\mathrm{d}yO(x,y)=I_oA_o$ and $\mathrm{std}(I_{\mathrm{noise}}^s)=\sqrt{\frac{1}{K}\sum_{s=1}^{K}(I_{\mathrm{noise}}^s-\langle I_{\mathrm{noise}}^s\rangle)^2}=\sqrt{\frac{1}{K}\sum_{s=1}^{K}(\delta I_{\mathrm{noise}}^s)^2}$ denotes the standard deviation of the noise vector I_{noise}^s. From Eq. (3), it is obviously observed that the value $\mathrm{DSNR}_{\mathrm{GI}}$ of GI depends on the number density of photons illuminating the object plane I_o and the object's transmission area A_o.

When the measurement number K is large enough or the patterns $\Delta I_r^s(x,y)$ conform to an orthogonal statistical distribution [namely the inner product of any two speckles $\Delta I_r^s(x,y)$ is zero and the mean value of $\Delta I_r^s(x,y)$ is also zero], Eq. (1) can be simplified as

$$O_{\mathrm{GI}}(x,y)$$
$$=\frac{1}{K}\sum_{s=1}^{K}\Delta I_r^s(x,y)(I_{\mathrm{signal}}^s+I_{\mathrm{noise}}^s)$$
$$=\frac{1}{K}\sum_{s=1}^{K}\Delta I_r^s(x,y)\Delta I_{\mathrm{signal}}^s+\frac{1}{K}\sum_{s=1}^{K}I_r^s(x,y)\Delta I_{\mathrm{noise}}^s$$
$$=I_o^2\left[O(x,y)\otimes\mu(x,y)+\frac{A_o}{K}\sum_{s=1}^{K}\frac{I_r^s(x,y)}{I_o}\frac{\mathrm{std}(I_{\mathrm{noise}}^s)}{\langle I_{\mathrm{signal}}^s\rangle}f^s\right]$$
$$\approx I_o^2\left[O(x,y)\otimes\mu(x,y)+\frac{\sqrt{A_o}}{K\sqrt{I_o}}\sum_{s=1}^{K}\frac{I_r^s(x,y)}{I_o}f^s\right]$$
$$=I_o^2\left[O(x,y)\otimes\mu(x,y)+\frac{\sqrt{A_o}}{\sqrt{I_o}}N(x,y)\right], \tag{4}$$

where $\mu(x,y)=\frac{\langle\Delta I_r^s(x,y)\Delta I_{\mathrm{signal}}^s\rangle}{\langle I_r^s(x,y)\rangle\langle I_{\mathrm{signal}}^s\rangle}$ denotes the coherence function of the two signals and $\otimes$ denotes the convolution symbol. $f_s=\delta I_{\mathrm{noise}}^s/\mathrm{std}(I_{\mathrm{noise}}^s)$ is approximately a noise vector with the mean value 0 and the standard deviation value 1, and $N(x,y)=\frac{1}{K}\sum_{s=1}^{K}\frac{I_r^s(x,y)}{I_o}f_s$. From Eq. (4), it is clearly seen that the first term of Eq. (4) corresponds to the object's image and the spatial resolution of GI is determined by the function $\mu(x,y)$. The second term of Eq. (4) represents a random noise image, which will cause a degradation of GI quality. In addition, because the amplitude of the noise image is $\frac{\sqrt{A_o}}{\sqrt{I_o}}$, the imaging SNR of GI will decrease as the object's transmission area A_o is increased, and increase with the photon number density I_o when only the photon shot noise of the detection system is considered, which is similar to the theoretical results of GI with a Gaussian speckle field[22].

The imaging SNR of the object's transmission region $\mathrm{SNR}_{\mathrm{GI}}^{\mathrm{tran}}$ for GI can be defined as

$$\mathrm{SNR}_{\mathrm{GI}}^{\mathrm{tran}}=10\times\log_{10}\left[\frac{\bar{O}_{\mathrm{GI}}^{\mathrm{tran}}}{\delta(O_{\mathrm{GI}}^{\mathrm{tran}})}\right], \tag{5}$$

where $\delta(O_{\mathrm{GI}}^{\mathrm{tran}}) = \sqrt{\frac{1}{N_x N_y}\sum_x^{N_x}\sum_y^{N_y}[O_{\mathrm{GI}}^{\mathrm{tran}}(x,y) - \bar{O}_{\mathrm{GI}}^{\mathrm{tran}}]^2}$ and $\bar{O}_{\mathrm{GI}}^{\mathrm{tran}} = \frac{1}{N_x N_y}\sum_x^{N_x}\sum_y^{N_y} O_{\mathrm{GI}}^{\mathrm{tran}}(x,y)$ are the standard deviation and mean value of the reconstructed object's transmission region in the spatial domain, respectively.

Conventional imaging is based on the point-to-point information extraction mode, and thus the imaging SNR is also equal to the system's DSNR. In comparison with GI, for the schematic shown in Fig. 1(b), if only the photon shot noise of the detection system is considered, then the imaging SNR of the object's transmission region $\mathrm{SNR}_{\mathrm{CI}}^{\mathrm{tran}}$ can be expressed as

$$\mathrm{DSNR}_{\mathrm{CI}} = \mathrm{SNR}_{\mathrm{CI}}^{\mathrm{tran}} = 10 \times \log_{10}(\sqrt{I_{\mathrm{photon}}}), \qquad (6)$$

where I_{photon} is the photon number received by the CCD camera at each pixel. In addition, Eq. (6) suggests that both $\mathrm{DSNR}_{\mathrm{CI}}$ and $\mathrm{SNR}_{\mathrm{CI}}^{\mathrm{tran}}$ of CI increase with $\sqrt{I_{\mathrm{photon}}}$.

To verify the analytical results, the parameters of the numerical simulation based on the schematic of Fig. 1 are set as follows: the wavelength of the laser is 532 nm and the transverse size of the laser beam illuminating the DMD is 10 mm by a conventional imaging system with the magnification 4×. The modulated area of the DMD is 64×64 pixels and the speckle's transverse size is set as 54.6 μm. The speckles modulated by the DMD are Hadamard patterns and the measurement number $K = 4096$, and thus the average number density of photons illuminating the DMD or the reflecting mirror is $I_0 = I_{\mathrm{photon}} = 2I_o$ for the demonstration of the performance comparison between CI and GI. In addition, $z_{t1} = z_{t2} = z_{r1} = z_{r2} = 200$ mm, $f_t = f_r = 100$ mm, and the transmission apertures of both the lenses f_t and f_r are 25 mm. For the image reconstruction of GI, we have used the intensity fluctuation correlation reconstruction algorithm[24]. When the object's transmission area is $A_o = 20 \times 20$ pixels^2, Figs. 2(a) and 2(b) illustrate the relationship between the value $\mathrm{DSNR}/\mathrm{SNR}^{\mathrm{tran}}$ and I_0 for both CI and GI. The imaging results of both CI and GI are shown in Figs. 2(c)–2(f) when the number density of photons illuminating the DMD is $I_0 = 1, 10, 100$, and 1000 photons/pixels^2, respectively. If I_0 is fixed at 40 photons/pixels^2, the DSNR and $\mathrm{SNR}^{\mathrm{tran}}$ on the object's transmission area A_o are shown in Fig. 3. From Figs. 2 and 3, it is obviously observed that for CI the values of both $\mathrm{DSNR}_{\mathrm{CI}}$ and $\mathrm{SNR}_{\mathrm{CI}}^{\mathrm{tran}}$ increase with $\sqrt{I_0}$ and do not depend on A_o, whereas the value $\mathrm{DSNR}_{\mathrm{GI}}$ is proportional to $\sqrt{I_o A_o}$ for GI. What is more, the value of $\mathrm{SNR}_{\mathrm{GI}}^{\mathrm{tran}}$ increases with $\sqrt{I_o}$ but is reduced with the increase of $\sqrt{A_o}$. Such simulation results displayed in Figs. 2 and 3 agree with the theoretical prediction described by Eqs. (3)–(6). In addition, the results shown in Figs. 3(b) and 3(f) also suggest that the imaging quality of CI will be better than that of GI when the object's transmission area A_o is beyond a threshold value $A_o^{\mathrm{threshold}}$ [for example, $A_o^{\mathrm{threshold}} = 2000$ pixels^2 in Fig. 3(b)].

In order to further clarify the performance differences between CI and GI, Fig. 4 presents $\mathrm{SNR}_{\mathrm{GI}}^{\mathrm{tran}}$ and

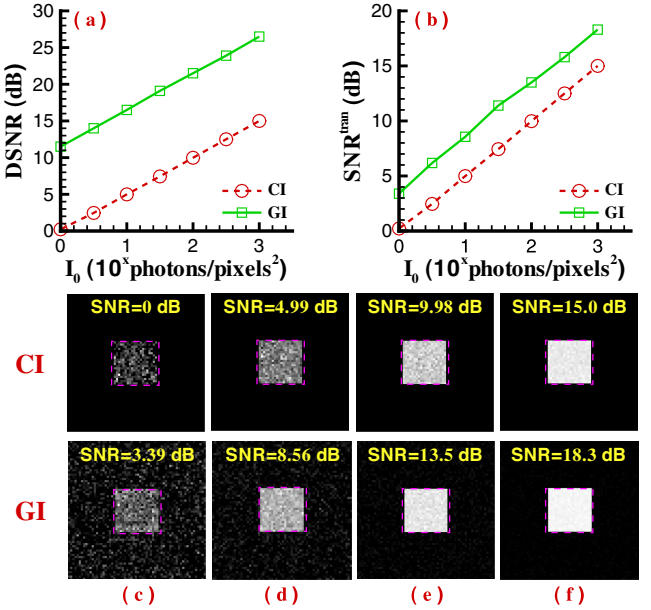

Fig. 2. Simulated results of CI and GI at different I_0 when the object's transmission area $A_o = 20 \times 20$ pixels^2 is fixed. (a) The relationship between the DSNR of CI/GI and the number density of photons illuminating the DMD or the reflection mirror I_0 ($I_0 = 2I_o$); (b) the dependence of the $\mathrm{SNR}^{\mathrm{tran}}$ of CI/GI on I_0; (c)–(f) the imaging results of CI and GI when $I_0 = 1$, 3, 10, and 30 photons/pixels^2, respectively. The areas shown by the pink dashed box in (c)–(f) correspond to the object's transmission region achieved by CI and GI.

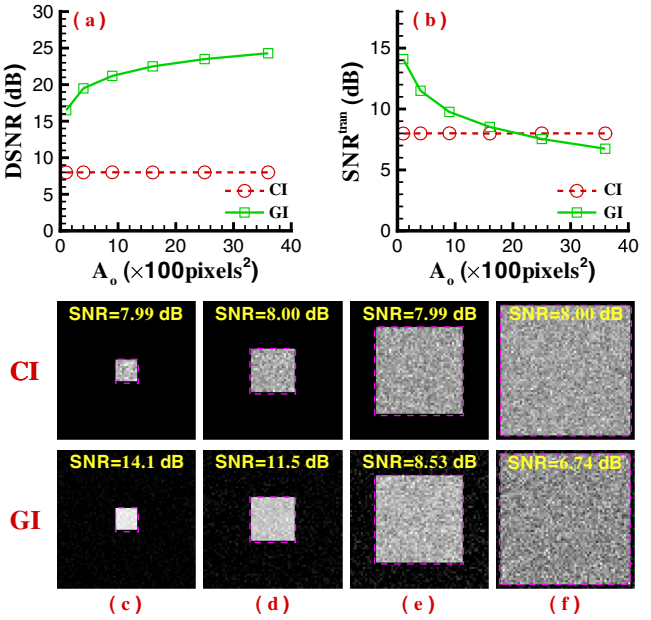

Fig. 3. Simulated results of CI and GI at different A_o in the case of $I_0 = 40$ photons/pixels^2. (a) The relationship between the DSNR of CI/GI and the object's transmission area A_o; (b) the dependence of the $\mathrm{SNR}^{\mathrm{tran}}$ of CI/GI on A_o; (c)–(f) the imaging results of CI and GI when $A_o = 100$, 400, 1600, and 3600 pixels^2, respectively. The areas labeled by the pink dashed box in (c)–(f) correspond to the object's transmission region achieved by CI and GI.

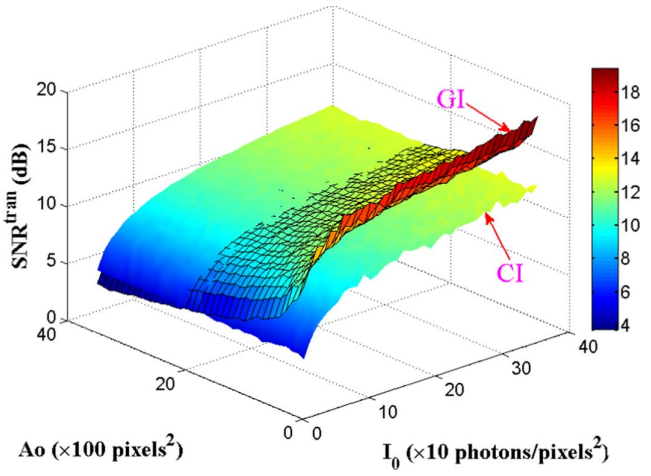

Fig. 4. Performance comparison of $\mathrm{SNR}^{\mathrm{tran}}$ for CI and GI for different I_0 and A_o.

$\mathrm{SNR}_{\mathrm{CI}}^{\mathrm{tran}}$ for different I_0 and A_o. From Fig. 4, we find that if $A_o > A_o^{\mathrm{threshold}} = 2000$ pixels^2, the value $\mathrm{SNR}_{\mathrm{CI}}^{\mathrm{tran}}$ will be always greater than that of GI and the influence of the photon number density I_0 on $\mathrm{SNR}_{\mathrm{CI}}^{\mathrm{tran}}$ and $\mathrm{SNR}_{\mathrm{GI}}^{\mathrm{tran}}$ is displayed in Fig. 5 when $A_o = 2000$ pixels^2 is fixed. It is clearly seen that if $A_o = A_o^{\mathrm{threshold}}$, both the imaging quality [see Figs. 5(c)–5(g)] and $\mathrm{SNR}^{\mathrm{tran}}$ [see Fig. 5(b)] of CI and GI are equivalent for the same I_0. Furthermore, as shown in Fig. 6, for the diagonal value of $\mathrm{SNR}^{\mathrm{tran}}$ of GI [see Figs. 4 and 6(a)], the value of $\mathrm{SNR}_{\mathrm{GI}}^{\mathrm{tran}}$ is also the same if $\frac{A_o}{I_o}$ maintains a constant value, which can be explained by

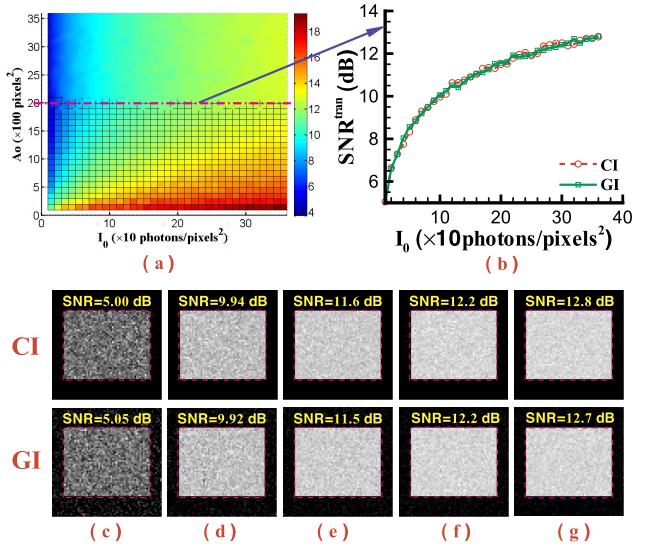

Fig. 5. The dependence of CI and GI on $\mathrm{SNR}^{\mathrm{tran}}$ for different I_0 when the threshold value $A_o^{\mathrm{threshold}}$ is chosen as 2000 pixels^2. (a) The projection diagram of $\mathrm{SNR}^{\mathrm{tran}}$ based on Fig. 4; (b) the curves of $\mathrm{SNR}^{\mathrm{tran}} - I_0$ for CI and GI corresponding to the pink dash-dotted line of (a); (c)–(g) the imaging results of CI and GI when $I_0 = 10$, 100, 200, 280, and 360 photons/pixels^2, respectively. The areas labeled by the pink dashed box in (c)–(g) correspond to the object's transmission region achieved by CI and GI.

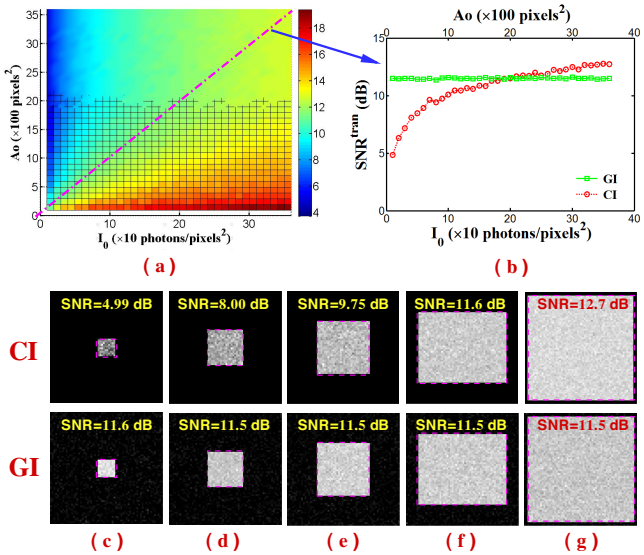

Fig. 6. Performance comparison of $\mathrm{SNR}^{\mathrm{tran}}$ for CI and GI for different I_0 and A_o, which correspond to the diagonal value of $\mathrm{SNR}^{\mathrm{tran}}$ in Fig. 4. (a) The projection diagram of $\mathrm{SNR}^{\mathrm{tran}}$ based on Fig. 4; (b) the $\mathrm{SNR}^{\mathrm{tran}}$ of CI and GI in the case of $\frac{A_o}{I_0} = 10$, corresponding to the pink dash-dotted line of (a); (c)–(g) the imaging results of CI and GI when $I_0 = 10$ photons/pixels^2 and $A_o = 10 \times 10$ pixels^2, $I_0 = 40$ photons/pixels^2 and $A_o = 20 \times 20$ pixels^2, $I_0 = 90$ photons/pixels^2 and $A_o = 30 \times 30$ pixels^2, $I_0 = 200$ photons/pixels^2 and $A_o = 40 \times 50$ pixels^2, and $I_0 = 360$ photons/pixels^2 and $A_o = 60 \times 60$ pixels^2, respectively. The areas labeled by the pink dashed box in (c)–(g) correspond to the object's transmission region achieved by CI and GI.

Eq. (4) and means that imaging an object with a large transmission area needs a much higher $\mathrm{DSNR}_{\mathrm{GI}}$ compared with imaging an object with a small transmission area [see Eq. (4)]. Therefore, in order to obtain the same $\mathrm{SNR}_{\mathrm{GI}}^{\mathrm{tran}}$ for two objects with the transmission areas A_1 and A_2, based on Eq. (3) and Eq. (4), the $\mathrm{DSNR}_{\mathrm{GI}}$ should satisfy $\mathrm{DSNR}_{A_1}/\mathrm{DSNR}_{A_2} = \sqrt{A_1/A_2}$. In addition, although we have used Hadamard patterns to illuminate the object for GI, Eq. (4) is universal and the results described above can be applied to GI with any random pattern.

In conclusion, the defined $\mathrm{SNR}^{\mathrm{tran}}$ is valid to evaluate the imaging quality of both GI and CI for a transmission object. Both the analytical and simulated results have shown that for CI the value $\mathrm{DSNR}_{\mathrm{CI}}$, which is the same as $\mathrm{SNR}_{\mathrm{CI}}^{\mathrm{tran}}$, increases with $\sqrt{I_0}$ and does not depend on A_o, whereas the $\mathrm{DSNR}_{\mathrm{GI}}$ is proportional to $\sqrt{I_o A_o}$ for GI. What is more, the $\mathrm{SNR}_{\mathrm{GI}}^{\mathrm{tran}}$ will be enhanced as I_o is increased but reduced with the increase of A_o. In addition, we can obtain the same $\mathrm{SNR}_{\mathrm{GI}}^{\mathrm{tran}}$ when $\frac{A_o}{I_o}$ maintains a constant value, and $\mathrm{SNR}_{\mathrm{CI}}^{\mathrm{tran}}$ will be larger than $\mathrm{SNR}_{\mathrm{GI}}^{\mathrm{tran}}$ when A_o is beyond a threshold value. Such results are helpful for the solution selection of GI and CI in practical applications.

This work was supported by the Youth Innovation Promotion Association of the Chinese Academy of Sciences

and the Defense Industrial Technology Development Program of China (No. D040301).

References

1. J. Cheng and S. Han, Phys. Rev. Lett. **92**, 093903 (2004).
2. R. S. Bennink, S. J. Bentley, R. W. Boyd, and J. C. Howell, Phys. Rev. Lett. **92**, 033601 (2004).
3. D. Z. Cao, J. Xiong, and K. Wang, Phys. Rev. A **71**, 013801 (2005).
4. M. D. Angelo and Y. H. Shih, Laser Phys. Lett. **2**, 567 (2005).
5. A. Gatti, M. Bache, D. Magatti, E. Brambilla, F. Ferri, and L. A. Lugiato, J. Mod. Opt. **53**, 739 (2006).
6. Y. Bromberg, O. Katz, and Y. Silberberg, Phys. Rev. A **79**, 053840 (2009).
7. C. Zhao, W. Gong, M. Chen, E. Li, H. Wang, W. Xu, and S. Han, Appl. Phys. Lett. **101**, 141123 (2012).
8. C. Wang, X. Mei, L. Pan, P. Wang, W. Li, X. Gao, Z. Bo, M. Chen, W. Gong, and S. Han, Remote Sens. **10**, 732 (2018).
9. C. Deng, L. Pan, C. Wang, X. Gao, W. Gong, and S. Han, Photon. Res. **5**, 431 (2017).
10. H. Yu, R. Lu, S. Han, H. Xie, G. Du, T. Xiao, and D. Zhu, Phys. Rev. Lett. **117**, 113901 (2016).
11. A. Zhang, Y. He, L.-A. Wu, L. Chen, and B. Wang, Optica **5**, 374 (2018).
12. W. Gong, C. Zhao, J. Jiao, E. Li, M. Chen, H. Wang, W. Xu, and S. Han, Sci. Rep. **6**, 26133 (2016).
13. M. Sun, M. P. Edgar, G. M. Gibson, B. Sun, N. Radwell, R. Lamb, and M. J. Padgett, Nat. Commun. **7**, 12010 (2016).
14. W. Gong and S. Han. Sci. Rep. **5**, 9280 (2015).
15. X. Chen, F. Kong, Q. Fu, S. Meng, and L-A. Wu, Opt. Lett. **42**, 5290 (2017).
16. J. Shi, G. Patera, Y. Gui, M. I. Kolobov, D. B. Horoshko, and S. Han, Chin. Opt. Lett. **16**, 092701 (2018).
17. H. Guo, R. He, C. Wei, Z. Lin, L. Wang, and S. Zhao, Chin. Opt. Lett. **17**, 071101 (2019).
18. H. Liu and S. Zhang, Appl. Phys. Lett. **111**, 031110 (2017).
19. R. I. Stantchev, B. Sun, S. M. Hornett, P. Hobson, G. M. Gibson, M. J. Padgett, and E. Hendry. Sci. Adv. **2**, e1600190 (2016).
20. X. Wang and Z. Lin, IEEE Trans. Geosci. Remote Sens. **56**, 4747 (2018).
21. F. Ferri, D. Magatti, L. A. Lugiato, and A. Gatti, Phys. Rev. Lett. **104**, 253603 (2010).
22. B. I. Erkmen and J. H. Shapiro, Adv. Opt. Photonics **2**, 405 (2010).
23. C. Wang, W. Gong, X. Shao, and S. Han, J. Opt. **18**, 065703 (2016).
24. W. Gong and S. Han, Phys. Lett. A **374**, 1005 (2010).